MOLECULAR ONCOLOGY 10 (2016) 866–878

available at www.sciencedirect.com

ScienceDirect

www.elsevier.com/locate/molonc

Glutathione biosynthesis is upregulated at the initiation of MYCN-driven neuroblastoma tumorigenesis

Daniel R. Carter[a,b,1], Selina K. Sutton[a,1], Marina Pajic[c,d], Jayne Murray[a], Eric O. Sekyere[e], Jamie Fletcher[a], Anneleen Beckers[f], Katleen De Preter[f], Frank Speleman[f], Rani E. George[g], Michelle Haber[a], Murray D. Norris[a,h], Belamy B. Cheung[a,b,*,2], Glenn M. Marshall[a,i,**,2]

[a]Children's Cancer Institute, Lowy Cancer Research Centre, University of New South Wales, Randwick 2031, Australia
[b]School of Women's & Children's Health, UNSW Australia, Randwick, New South Wales 2031, Australia
[c]The Kinghorn Cancer Centre, Cancer Division, Garvan Institute of Medical Research, University of New South Wales, 384 Victoria St, Darlinghurst, Sydney, New South Wales 2010, Australia
[d]St Vincent's Clinical School, Faculty of Medicine, University of New South Wales, New South Wales 2010, Australia
[e]Endeavour College of Natural Health, Sydney, 2000, Australia
[f]Center for Medical Genetics (CMGG), Ghent University, Medical Research Building (MRB1), De Pintelaan 185, 9000 Ghent, Belgium
[g]Department of Pediatric Hematology and Oncology, Dana-Farber Cancer Institute and Boston Children's Hospital, Harvard Medical School, Boston, MA, USA
[h]University of New South Wales, Centre for Childhood Cancer Research, Randwick, New South Wales 2031, Australia
[i]Kids Cancer Centre, Sydney Children's Hospital, Randwick 2031, Australia

ARTICLE INFO

Article history:
Received 14 December 2015
Received in revised form
11 February 2016
Accepted 19 February 2016
Available online 2 March 2016

ABSTRACT

The MYCN gene is amplified and overexpressed in a large proportion of high stage neuroblastoma patients and has been identified as a key driver of tumorigenesis. However, the mechanism by which MYCN promotes tumor initiation is poorly understood. Here we conducted metabolic profiling of pre-malignant sympathetic ganglia and tumors derived from the *TH-MYCN* mouse model of neuroblastoma, compared to non-malignant ganglia from wildtype littermates. We found that metabolites involved in the biosynthesis of glutathione, the most abundant cellular antioxidant, were the most significantly upregulated

Abbreviations: MYCN, V-Myc Avian Myelocytomatosis Viral Oncogene Neuroblastoma Derived Homolog; *TH-MYCN*, Transgenic mouse strain that overexpresses MYCN conditionally in sympathetic tissues under the control of tyrosine hydroxylase promoter; HIF, Heat-shock inducible factor; PKM2, Pyruvate kinase isozyme M2; NADPH, Reduced nicotinamide adenine dinucleotide phosphate; ROS, Reactive oxygen species; MSEA, Metabolite set enrichment analysis; NET AUC^{MYCN}, The net area under curve value for *TH-MYCN* samples; GSEA, Gene set enrichment analysis; H_2O_2, Hydrogen peroxide; BSO, Buthionine sulfoximine; BPTES, Bis-2-(5-phenylacetamido-1,2,4-thiadiazol-2-yl)ethyl sulfide 3.

* *Corresponding author*. Children's Cancer Institute, Lowy Cancer Research Centre, University of New South Wales, Randwick 2031, Australia.
** *Corresponding author*. Children's Cancer Institute, Lowy Cancer Research Centre, University of New South Wales, Randwick 2031, Australia.
E-mail addresses: BCheung@ccia.unsw.edu.au (B.B. Cheung), g.marshall@unsw.edu.au (G.M. Marshall).
[1] Equal first authors.
[2] Equal corresponding authors

http://dx.doi.org/10.1016/j.molonc.2016.02.004

Keywords:
Neuroblastoma
MYCN
Glutathione
Metabolomics
Tumorigenesis
BSO

metabolic pathway at tumor initiation, and progressively increased to meet the demands of tumorigenesis. A corresponding increase in the expression of genes involved in ribosomal biogenesis suggested that MYCN-driven transactivation of the protein biosynthetic machinery generated the necessary substrates to drive glutathione biosynthesis. Premalignant sympathetic ganglia from *TH-MYCN* mice had higher antioxidant capacity and required glutathione upregulation for cell survival, when compared to wildtype ganglia. Moreover, *in vivo* administration of inhibitors of glutathione biosynthesis significantly delayed tumorigenesis when administered prophylactically and potentiated the anticancer activity of cytotoxic chemotherapy against established tumors. Together these results identify enhanced glutathione biosynthesis as a selective metabolic adaptation required for initiation of MYCN-driven neuroblastoma, and suggest that glutathione-targeted agents may be used as a potential preventative strategy, or as an adjuvant to existing chemotherapies in established disease.

1. Introduction

Neuroblastoma is a pediatric embryonal malignancy of the sympathetic nervous system (Brodeur, 2003; Maris, 2010). Amplification of the V-Myc Avian Myelocytomatosis Viral Oncogene Neuroblastoma Derived Homolog (*MYCN*) gene locus occurs in approximately 20% of patients and predicts poor prognosis (Maris, 2010; Schwab et al., 1983). *MYCN* amplification leads to high-level MYCN expression, leading to aberrant transcriptional activation and repression of genes that support a malignant phenotype (Brodeur, 2003; Brodeur et al., 1984; Maris, 2010; Schwab et al., 1983, 1984). In the normal embryo, MYCN expression is high in the early post-migratory neural crest where it regulates the early sympathoadrenal lineage but it is gradually down-regulated and is generally expressed at low levels through postnatal life (Zimmerman et al., 1986). The causal role of MYCN expression in neuroblastoma tumorigenesis is supported by the observation that sympathetic tissue-specific expression of the human *MYCN* gene in *TH-MYCN* transgenic mice causes a murine equivalent of neuroblastoma that recapitulates almost all of the features of the human disease (Chesler and Weiss, 2011; Weiss et al., 1997). Currently, direct MYCN-targeted agents have not been developed, but there has been recent preclinical success with indirect treatment approaches that inhibit MYCN by targeting its expression, protein stability or transcriptional activity (Brockmann et al., 2013; Carter et al., 2015; Chipumuro et al., 2014; Puissant et al., 2013). This suggests that indirect targeting strategies show significant promise for MYCN-amplified neuroblastoma patients.

Sympathetic ganglia in *TH-MYCN* mice exhibit hyperplasia of sympathetic progenitors, or neuroblasts, prior to malignant transformation (Alam et al., 2009; Calao et al., 2012; Hansford et al., 2004). In humans, a similar population of remnant neuroblasts termed "neuroblastoma *in situ*", has been described in the adrenal medulla of infants at a much higher incidence than clinical neuroblastoma (Beckwith and Perrin, 1963). Together this suggests that neuroblastoma initiates from remnant cells of the embryonic sympathoadrenal lineage which have pathologically persisted postnatally (Marshall et al., 2014). Persistent neuroblasts in neuroblastoma tumor initiation develop resistance mechanisms to differentiation or deletion signals normally received by prenatal cells produced in excess to requirements for organogenesis (Calao et al., 2012; Hansford et al., 2004; Marshall et al., 2014). In *TH-MYCN* mouse ganglia the majority of hyperplastic neuroblasts also spontaneously regress prior to later tumorigenesis (Hansford et al., 2004). Tumors must therefore arise from clonally selected cells with secondary pro-survival characteristics.

Metabolism in cancer cells is fundamentally altered to meet the demands of malignancy. As cancer cells rapidly proliferate, metabolism must be altered to sustain adequate macromolecule biosynthesis, energy production and redox balance (Cairns et al., 2011). Moreover, in large solid tumors such as neuroblastoma, a unique micro-environment dictates that tumor cells often need to survive avascular conditions during tumor progression and develop resistance mechanisms to oxygen deprivation (Mohlin et al., 2015). Recent evidence in mouse models of some adult cancers also suggests that cancer-specific changes in metabolic pathways, such as those that maintain redox balance, are essential for the earliest stages of tumor initiation (Harris et al., 2015).

MYCN and family member MYC have been closely tied to the regulation of a plethora of metabolic pathways in cancer (Cairns et al., 2011; Dang et al., 2009). MYC collaborates with heat-shock inducible factor (HIF) proteins to promote glucose uptake and glycolytic flux by direct transcriptional regulation of glucose transporters and glycolytic enzymes (Dang et al., 2008; Kim et al., 2007). Moreover, MYC can support the macromolecular demand of rapidly dividing cancer cells by driving preferential pyruvate kinase isozyme M2 (PKM2) expression and pentose phosphate pathway activation (David et al., 2010). MYC-driven tumors enhance glutamine transport and glutamate metabolism to support flux through the citric acid cycle which provides the carbon backbone required for macromolecule biosynthesis (Le et al., 2012). MYC has also been linked to altered redox control by enhancing production of antioxidants, glutathione and reduced nicotinamide adenine dinucleotide phosphate (NAPDH) to overcome potentially damaging metabolic byproducts, such as reactive oxygen

species (ROS) (Cairns et al., 2011; David et al., 2010; Gao et al., 2009; Veas-Perez de Tudela et al., 2010).

To evaluate specific metabolic changes in MYCN-driven neuroblastoma tumorigenesis, we have conducted a metabolomics analysis on sympathetic ganglia and tumor tissues derived from *TH-MYCN* mice. We show that glutathione biosynthesis is specifically upregulated during *TH-MYCN* tumorigenesis compared to normal tissues. This occurred due to an over-abundance of upstream substrates driving glutathione biosynthesis pathway activation. Moreover, we show that glutathione depletion is selectively toxic to pre-malignant *TH-MYCN* ganglia cells and inhibits MYCN-driven tumorigenesis.

2. Materials and methods

2.1. Isolation of ganglia/tumors for metabolomics

A transgenic mouse model of neuroblastoma that overexpresses human MYCN in the sympathetic lineage develops a murine equivalent of human neuroblastoma as previously described (Weiss et al., 1997). Sympathetic ganglia (pooled cervical ganglia and coeliac ganglia) or tumors were dissected from 2, 4 and 6 week wild-type and *TH-MYCN*$^{+/+}$ mice as previously described (Calao et al., 2012; Carter et al., 2015; Hansford et al., 2004) and washed in Hanks balanced salt solution and snap-frozen. Metabolic analyses were performed in duplicate for wild-type and *TH-MYCN*$^{+/+}$ mice (from 2 to 3 pooled samples/time point). All subsequent steps in metabolic profiling were normalized to the mass of each sample.

2.2. Metabolic profiling

2.2.1. Metabolite analysis

Metabolomics profiling analysis was performed by Metabolon as previously described (Reitman et al., 2011).

2.2.2. Sample preparation

Samples were prepared using the automated MicroLab STAR® system from Hamilton Company. A recovery standard was added prior to the first step in the extraction process for the purpose of quality control. Sample preparation was conducted using an aqueous methanol extraction process to remove the protein fraction while allowing maximum recovery of small molecules. The resulting extract was divided into four fractions: one for analysis by UPLC/MS/MS (positive mode), one for UPLC/MS/MS (negative mode), one for GC/MS, and one for contingency. Samples were placed briefly on a TurboVap® (Zymark) to remove the organic solvent. Each sample was then frozen and dried under vacuum. Samples were then prepared for the appropriate instrument, either UPLC/MS/MS or GC/MS.

2.2.3. Ultrahigh performance liquid chromatography/mass spectroscopy (UPLC/MS/MS)

The LC/MS portion of the platform was based on a Waters ACQUITY ultra-performance liquid chromatography (UPLC) and a Thermo-Finnigan linear trap quadrupole (LTQ) mass spectrometer, which consisted of an electrospray ionization (ESI) source and linear ion-trap (LIT) mass analyzer. The sample extract was dried then reconstituted in acidic or basic LC-compatible solvents, each of which contained 8 or more injection standards at fixed concentrations to ensure injection and chromatographic consistency. One aliquot was analyzed using acidic positive ion optimized conditions and the other using basic negative ion optimized conditions in two independent injections using separate dedicated columns. Extracts reconstituted in acidic conditions were gradient eluted using water and methanol containing 0.1% formic acid, while the basic extracts, which also used water/methanol, contained 6.5 mM Ammonium Bicarbonate. The MS analysis alternated between MS and data-dependent MS2 scans using dynamic exclusion. Raw data files are archived and extracted as described below.

2.2.4. Gas chromatography/mass spectroscopy (GC/MS)

The samples destined for GC/MS analysis were re-dried under vacuum desiccation for a minimum of 24 h prior to being derivatized under dried nitrogen using bistrimethyl-silyl-triflouroacetamide (BSTFA). The GC column was 5% phenyl and the temperature ramp was from 40° to 300 °C in a 16 min period. Samples were analyzed on a Thermo-Finnigan Trace DSQ fast-scanning single-quadrupole mass spectrometer using electron impact ionization. The instrument was tuned and calibrated for mass resolution and mass accuracy on a daily basis. The information output from the raw data files was automatically extracted as discussed below.

2.2.5. Quality assurance/quality control (QA/QC)

For QA/QC purposes, additional samples were included with each day's analysis. These samples included extracts of a pool of well-characterized human plasma, extracts of a pool created from a small aliquot of the experimental samples, and process blanks. QC samples were spaced evenly among the injections and all experimental samples were randomly distributed throughout the run. A selection of QC compounds was added to every sample for chromatographic alignment, including those under test. These compounds were carefully chosen so as not to interfere with the measurement of the endogenous compounds.

2.2.6. Data extraction and compound identification

Raw data was extracted, peak-identified and QC processed using Metabolon's hardware and software. These systems are built on a web-service platform utilizing Microsoft's.NET technologies, which run on high-performance application servers and fiber-channel storage arrays in clusters to provide active failover and load-balancing. Compounds were identified by comparison to library entries of purified standards or recurrent unknown entities. More than 2400 commercially available purified standard compounds have been acquired and registered into Metabolon's system for distribution to both the LC and GC platforms for determination of their analytical characteristics.

2.2.7. Metabolite quantitative analysis

The dataset was refined to include only metabolites that were detected in all samples and had a corresponding

human metabolome database identification number that was required for downstream analysis (n = 156). Area under curve analysis was conducted in R software using "auc" command of the MESS package. For heatmap analysis, raw data was normalized to week 2 wild-type ganglia and plotted according to the "heatmap.2" command of the ggplots package.

2.3. Metabolite set enrichment analysis (MSEA)

MSEA was conducted as previously described on the dedicated web-based platform (http://www.msea.ca/MSEA/) (Xia and Wishart, 2010). Specifically the top 50 metabolites ranked by net area under curve in *TH-MYCN* ganglia/tumors compared to wild-type ganglia, were analyzed by over-representation analysis in 80 metabolic pathways of the Small Molecular Pathway Database (Frolkis et al., 2010; Xia and Wishart, 2010). Refer to Figure 1A and Results section for a more detailed explanation on the methodology used.

2.4. Gene set enrichment analysis

Coeliac and superior cervical ganglia were isolated from two-week old *TH-MYCN*$^{+/+}$ mice and wild-type littermates as previous described (Calao et al., 2012; Carter et al., 2015; Hansford et al., 2004). RNA was isolated and hybridized to Agilent SurePrint G3 Mouse GE 8 × 60K Microarrays. Arrays were normalized using GenePattern software (version 3.2.3 Broad Institute) using the AgilentToGCT and LimmaGP modules (version 19.3) available at https://pwbc.garvan.unsw.edu.au/gp. Gene expression data is available at the Gene Expression Omnibus accession #GSE71105. Gene set enrichment analysis (http://www.broadinstitute.org/gsea/index.jsp) (Mootha et al., 2003; Subramanian et al., 2005) was conducted on a pre-ranked list of differentially expressed genes in *TH-MYCN*$^{+/+}$ ganglia compared to wild-type ganglia. Gene sets for KEGG and GO target genes are available in the Molecular Signature Database (http://www.broadinstitute.org/gsea/msigdb/index.jsp).

2.5. Primary sympathetic ganglia cultures

Coeliac and superior cervical ganglia were isolated from two-week old *TH-MYCN*$^{+/+}$ mice and wild-type littermates and cultured as previous described (Calao et al., 2012; Carter et al., 2015; Hansford et al., 2004). Briefly, extracted ganglia were placed in Hanks' balanced salt solution (Life Technologies) containing 1 mg/ml collagenase (Sigma) at 4 °C for 30 min and then dissociated by adding 0.05% trypsin at 37 °C for 8–11 min. Samples were then washed twice, resuspended, and triturated in Neurobasal-A media (Life Technologies) supplemented with 0.5 mM L-glutamine, 25 μM glutamic acid, penicillin streptomycin (1% vol/vol), and B27 (Life Technologies; 2% vol/vol; complete media). Ganglia cells were cultured in complete Neurobasal-A media supplemented with 10% B27 (Life Technologies) on poly-D-lysine and laminin-coated coverslips in 8 well chamber slides (Lab-Tek II - Thermo Scientific) in the presence of NGF (50 ng/ml; Biosensis) and aphidicolin (3.3 μg/ml; Sigma). 48 h after seeding, ganglia cultures were then washed gently by dilution with PBS to avoid cell contact with air and media was replaced with whole growth media. Cultures were then incubated for 48 h and neural lineage cells were quantified by immunofluorescent staining for βIII-tubulin (see below). Data is expressed as the percentage of βIII-tubulin positive cells compared with untreated cells. Ganglia cultures treated with BSO (Sigma), H_2O_2 (Sigma), or, L-glutamine (Life technologies), and D-glucose (Sigma) supplementation was done so 48 h after seeding for a total of 48 h. All data is representative of three independent biological replicates ± standard error.

2.6. Immunofluorescence

Primary ganglia cultures in 8 well chamber slides were fixed in 3–4% paraformaldehyde for 15 min at room temperature followed by 30 min of 0.4–0.5% Triton-X to permeabilize cells. After washing with PBS, cells were then blocked with 10% FCS for 1 h, followed by overnight incubation with rabbit anti-βIII–tubulin (Covance 1:1000) at 4 °C in a humid environment. Secondary anti-rabbit-Alexa-Fluor 488 (Life Technologies 1:2000) was then incubated for 45 min at room temperature and slides were mounted with coverslips using DAPI mounting solution (Southern Biotech). DAPI was used to determine nuclear stain. βIII tubulin was used to determine the number of neural lineage cells. Cells were counted on the Zeiss Axioplan II microscope. Counts reflect all cells in a particular well normalized relative to control for three independent experiments.

2.7. BSO and BPTES prophylaxis in pre-tumor TH-MYCN mice

For prophylaxis studies, 2.5 mmol/kg BSO (Sigma), 12.5 mg/kg BPTES (Sigma) or 0.9% saline was administered intraperitoneally to *TH-MYCN*$^{+/-}$ mice at 6 days of age for a total of 5 days/once a day. Mice were then culled and fixed for H&E staining and histological analysis. All mice were examined for the proportion of ganglia which exhibited neuroblast hyperplasia. >30 neuroblasts/focal region in each ganglion were considered to be hyperplastic (Calao et al., 2012; Carter et al., 2015; Hansford et al., 2004). Data presented is the average proportion of ganglia which were hyperplastic ± standard error for each mouse. For examination of time to tumor onset, prophylactic BSO was administered by gavage at 500 mg/kg into 3 week old *TH-MYCN*$^{+/+}$ mice. They were continued on treatment, once per day until palpable tumors were detected. The Kaplan–Meier chart shows the age of mice when tumors were first detected (by palpation).

2.8. BSO and vincristine treatment in TH-MYCN mice with established tumors

Upon the development of 5 mm diameter tumors by palpation (~4–5 weeks old), *TH-MYCN*$^{+/+}$ transgenic mice were randomized into treatment groups to receive treatments. After which, mice were monitored until the development of a medium (~10 mm) palpable abdominal tumor or signs of thoracic tumor development (labored breathing or hind limb paralysis as previously described (Carter et al., 2015; Henderson et al., 2011)). For Kaplan–Meier analysis, a 10 mm palpable tumor is considered the survival endpoint.

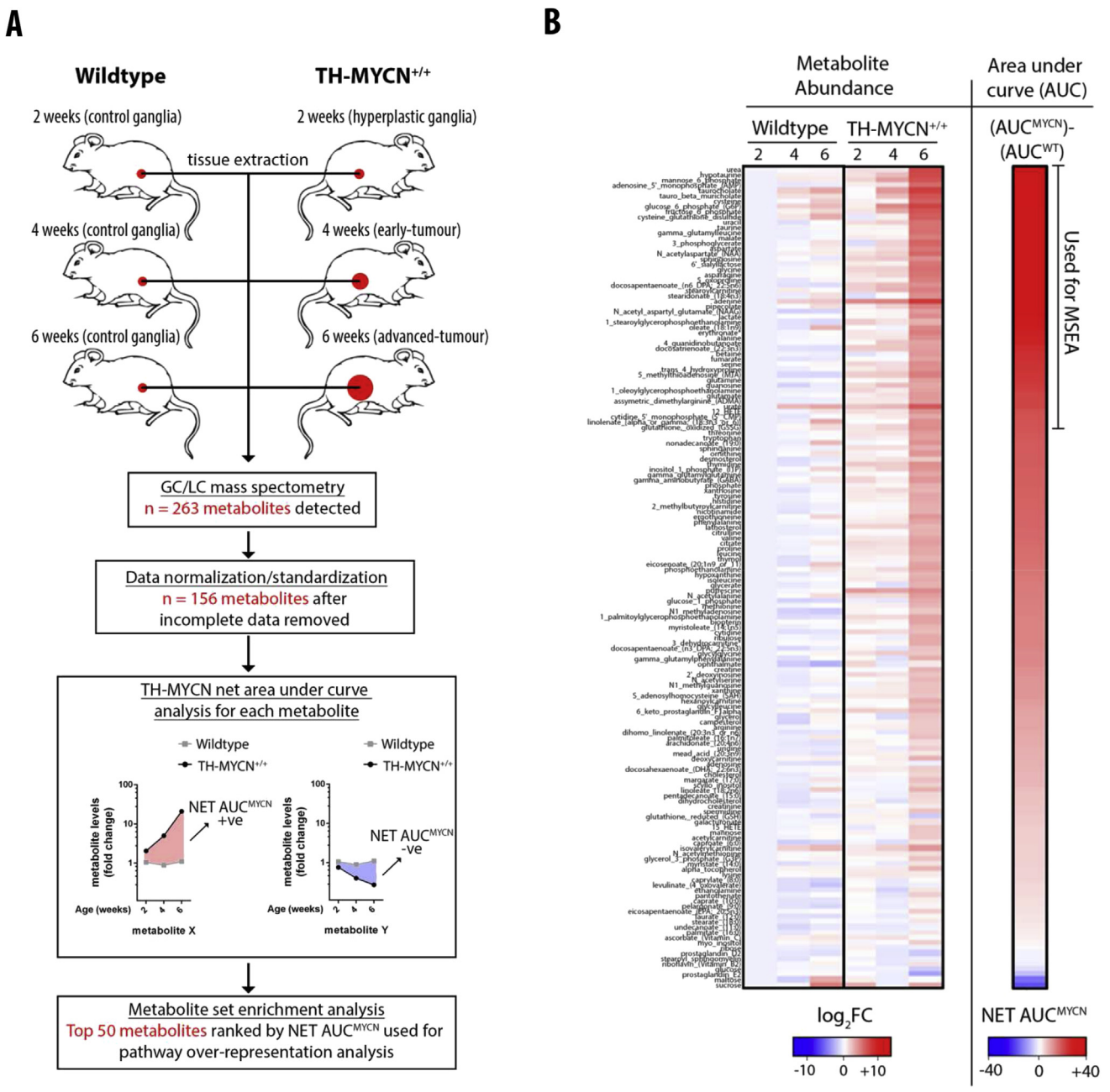

Figure 1 – Temporal analysis of metabolism through neuroblastoma tumorigenesis. A) Schematic of experimental plan used in the metabolic profiling for this study. Sympathetic ganglia and tumors from *TH-MYCN*$^{+/+}$ mice and age-matched wild-type littermates were dissected at the indicated ages for metabolic profiling. Metabolic profiling was conducted using gas chromatography (GS) or liquid chromatography (LS) and mass spectrometry (n = 263). After data normalization and standardization, abundance for each metabolite was quantified across multiple time points for each genotype using area under curve (AUC) analysis (n = 156). Net AUC^{MYCN} refers to the AUC value for each metabolite from *TH-MYCN* ganglia/tumors minus the AUC value for wild-type ganglia. The top 50 metabolites ranked by NET AUC^{MYCN} were subsequently used in metabolite set enrichment analysis to evaluate which pathways have metabolites that were over-represented. B) Heatmap representation of metabolite abundance expressed as log2 adjusted fold change (log_2FC) of the metabolite abundance detected in week 2 wild-type ganglia. NET AUC^{MYCN} heatmap values for each metabolite are also plotted. Data ranked from top to bottom by NET AUC^{MYCN} value. For full list of individual metabolite quantities, refer to Supplementary Table 1.

Percentage of mice developing tumors (y-axis) refers to the proportion of mice which have not reached endpoint at any given time (x-axis). Kaplan–Meier graphs were generated with GraphPad Prism 6 and two-sided log-rank tests were used to compare groups. In order to prevent severe constipation, animals treated with vincristine in the presence or absence of BSO were administered paraffin oil (100 μL) by gavage on two occasions during the experiment, and were also given additional supplementation with glutamic acid 0.1 mg/mL in drinking water.

For single agent BSO studies, mice received BSO at 500 mg/kg or saline by gavage for 5 consecutive days. For BSO/vincristine combination studies, BSO was administered at 500 mg/kg by gavage 4 h prior to intraperitoneal vincristine at 0.2 mg/kg. Treatment continued for a total of 5 days, once per day and then tumors were measured by palpation daily, until they reached 10 mm in diameter (i.e. the survival endpoint).

2.9. *Animal ethics*

All experimental animal procedures were approved by the University of New South Wales Animal Care and Ethics Committee according to the Animal Research Act, 1985 (New South Wales, Australia) and the Australian Code of Practice for Care and Use of Animals for Scientific Purposes (1997).

2.10. *Statistical analysis*

Area under curve and heatmap analysis were computed using R software. All comparisons of means were computed with two-sided t-tests in Graphpad Prism. Differences between non-linear regression curves were computed using extra sum of squares F-test in Graphpad Prism. Differences in survival proportions were computed using log-rank tests in Graphpad Prism. MSEA was conducted using the web-platform available at http://www.msea.ca/MSEA/by over-representation analysis on Small Molecular Pathway Database canonical metabolic pathways (Frolkis et al., 2010; Xia and Wishart, 2010). GSEA was conducted using standalone GSEA software available at http://software.broadinstitute.org/gsea/index.jsp.

3. Results

3.1. *Temporal analysis of metabolism through neuroblastoma tumorigenesis*

Since neuroblastoma tumorigenesis in the *TH-MYCN* mouse model is characterized by distinct phenotypic stages, we conducted a metabolomics analysis on sympathetic ganglia and tumor tissues isolated at multiple time points after birth and compared them to ganglia from wild-type littermates (Figure 1A). We collected tissues at postnatal 2, 4, and 6 weeks of age, which in the *TH-MYCN*$^{+/+}$ mice correspond to stages of ganglia hyperplasia (pre-tumor), early tumor (first palpable age: ~1–3 mm diameter) or an advanced tumor (~8–10 mm diameter), respectively (Hansford et al., 2004; Weiss et al., 1997). To quantify metabolites in these samples, we used liquid or gas chromatography coupled with mass spectrometry (Reitman et al., 2011). In total, 263 unique metabolites were matched to their respective standards in at least one sample and metabolites were quantified accordingly (Supplementary Table S1). We further refined the dataset to include only metabolites that were detected in all samples and had a corresponding human metabolome database identification number that was required for downstream analysis (n = 156) (Supplementary Table S2). With the refined dataset we then conducted area under curve (AUC) analysis for each analyte to quantify the magnitude of difference between metabolites in *TH-MYCN*$^{+/+}$ and wild-type samples over time. All metabolites were ranked by net AUC for *TH-MYCN*$^{+/+}$ mice (NET AUC^{MYCN}), i.e. each metabolites AUC for *TH-MYCN*$^{+/+}$ samples minus the AUC for wildtype samples (Supplementary Table S2, see Figure 1A for methodology). Heatmap analysis identified that the vast majority of tested metabolites were upregulated in *TH-MYCN*$^{+/+}$ ganglia/tumors when normalized by week 2 wild-type ganglia values (Figure 1B). NET AUC^{MYCN} demonstrated that 151/156 (96.8%) metabolites were upregulated to some degree in *TH-MYCN*$^{+/+}$ mice (NET AUC^{MYCN} >0) (Figure 1B, Supplementary Table S2).

3.2. *Glutathione biosynthesis is upregulated during* TH-MYCN$^{+/+}$ *tumorigenesis*

Considering that the vast majority of metabolites were upregulated in *TH-MYCN*$^{+/+}$ mice, we next evaluated which metabolic pathways were upregulated to the greatest degree. For this analysis we conducted metabolite set enrichment analysis (MSEA - http://www.msea.ca/MSEA/) (Xia and Wishart, 2010). Specifically, we examined whether the top 50 metabolites ranked by NET AUC^{MYCN} were over-represented among the 80 human metabolic pathways found in the Small Molecular Pathway Database (Supplementary Table S3) (Frolkis et al., 2010). This method produces a hypergeometric test score to evaluate relative pathway enrichment (i.e. the fold change in the number of metabolites present within the pathway over the number expected to be in the pathway) (Xia and Wishart, 2010). MSEA based on the top 50 metabolites ranked by NET AUC^{MYCN} showed that the most enriched metabolic pathway was glutathione metabolism (Figure 2A, Supplementary Table S4). Glutathione is the most abundant antioxidant within cells, and has been implicated as a key requirement to overcome oxidative stress in highly metabolic active cancer cells (Cairns et al., 2011). Notably, a number of metabolic pathways inter-related to glutathione metabolism were also enriched in the MSEA results, such as glutamate metabolism, glycine metabolism and cysteine metabolism (Figure 2A, asterisks), which would satisfy the substrate demand for glutathione biosynthesis. We next identified the patterns of increase in seven glutathione metabolism substrates and products, which were consistently upregulated in *TH-MYCN*$^{+/+}$ ganglia, compared to wild-type ganglia, over the course of tumorigenesis (Figure 2B). These patterns of change suggested that the biosynthetic arm of glutathione metabolism was upregulated at both initiation and later progression of the *TH-MYCN* tumorigenesis process.

3.3. *Glutathione biosynthesis is upregulated due to excessive upstream substrate abundance*

We next evaluated the mechanism by which MYCN enhanced glutathione biosynthesis in *TH-MYCN*$^{+/+}$ ganglia. As MYC proteins have been implicated in the regulation of a number of the enzymes required for glutathione biosynthesis (Benassi et al., 2006; Gao et al., 2009; Veas-Perez de Tudela et al., 2010; Xiao et al., 2015), we examined the expression of enzymes involved in this pathway from gene expression arrays of 2 week old *TH-MYCN*$^{+/+}$ and wild-type ganglia (Figure 3A). Surprisingly, we found that the mRNA expression levels of the glutathione

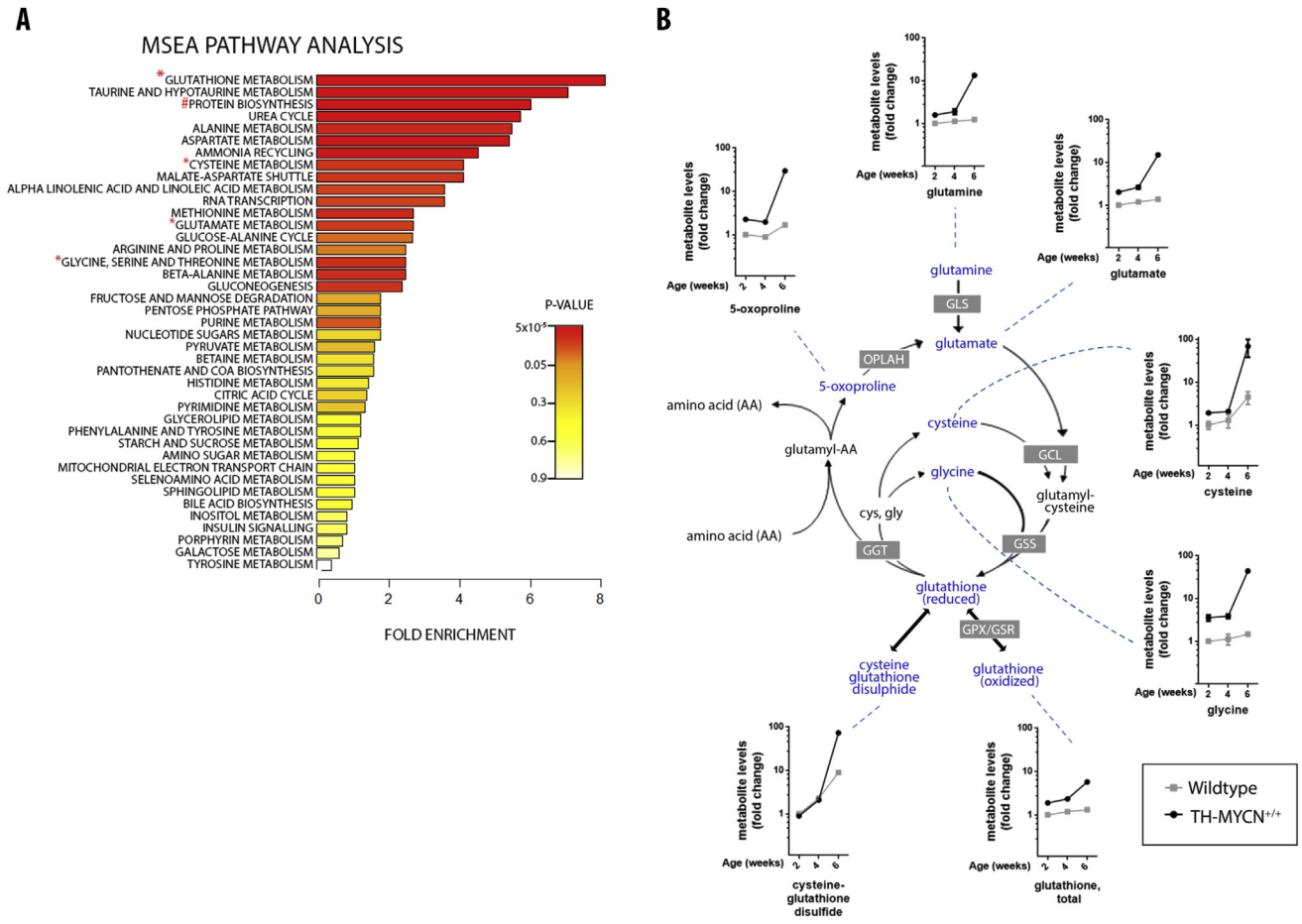

Figure 2 – Glutathione biosynthesis is upregulated in *TH-MYCN* mice through tumorigenesis. A) The top 50 metabolites ranked by NET AUC^{MYCN} were computed for over-representation by metabolite set enrichment analysis (MSEA) on 80 metabolic pathways of the small molecule pathway database (http://www.msea.ca/MSEA). Each pathway is quantified by a hypergemometric test score to evaluate to what extent metabolites were enriched in a pathway as compared to their expected enrichment by chance alone. * indicates pathways that relate to glutathione biosynthesis. # indicates the protein biosynthesis pathway. Only pathways with enrichment greater than 0 are shown. Refer to Supplementary Table S4 for full analysis. B) The metabolites of the glutathione biosynthesis pathway are displayed diagrammatically and are accompanied by their relative abundance in *TH-MYCN*$^{+/+}$ and wild-type samples. Enzymes involved in the pathway are also displayed. GLS, glutaminase, GCL, glutamyl-cysteine ligase, GPX, glutathione peroxidase, GSR, glutathione reductase, GGT, gamma-glutamyl transpeptidase, GSS; glutathione synthetase, OPLAH, 5-Oxoprolinase ATP-Hydrolyzing.

biosynthetic enzymes were mostly downregulated in *TH-MYCN*$^{+/+}$ ganglia and overall were significantly downregulated compared to other genes by gene set enrichment analysis (Figure 3A–B). This suggests that increased abundance of metabolites of the glutathione biosynthesis pathway was not driven by increased transcription of key enzymes. We therefore expanded our gene set enrichment analysis using expression arrays from 2 week old *TH-MYCN*$^{+/+}$ and wild-type ganglia to explore canonical pathways of the KEGG database (http://www.genome.jp/kegg/pathway.html) (Ogata et al., 1999) to discover alternative mechanisms of pathway upregulation. Numerous expected pathways were identified to be enriched in *TH-MYCN*$^{+/+}$ ganglia indicative of increased cell proliferation, such as those related to cell cycle/biogenesis and DNA repair (Figure 3C – asterisks and hashtags respectively, Supplementary Table 5). Interestingly though, genes involved in ribosome biogenesis were also highly enriched (Figure 3C – red box, Figure 3D, Supplementary Table 5). Ribosome biogenesis and regulation have been strongly linked to MYC proteins in cancer to meet the protein translational demands of cancer cells (van Riggelen et al., 2010). Upregulated ribosome biogenesis leads to overall increases in the total cellular amino acid pool, therefore, we explored the possibility that the glutathione biosynthesis pathway is driven by excessive abundance of upstream substrates. Consistent with our findings from KEGG pathways, gene ontology analysis on *TH-MYCN*$^{+/+}$ ganglia gene expression also showed upregulation of genes involved in ribosomal biogenesis compared to wildtype ganglia (Figure 3E). In accordance with this observation, we also found that the protein biosynthesis pathway was highly enriched in *TH-MYCN*$^{+/+}$ mice (Figure 2A, hashtag). Together these data support a hypothetical model whereby MYCN deregulation throughout neuroblastoma tumorigenesis leads to increased protein biosynthesis by transactivation of ribosomal genes, and consequently, excessive cysteine, glutamate and glycine abundance drives increased glutathione biosynthesis.

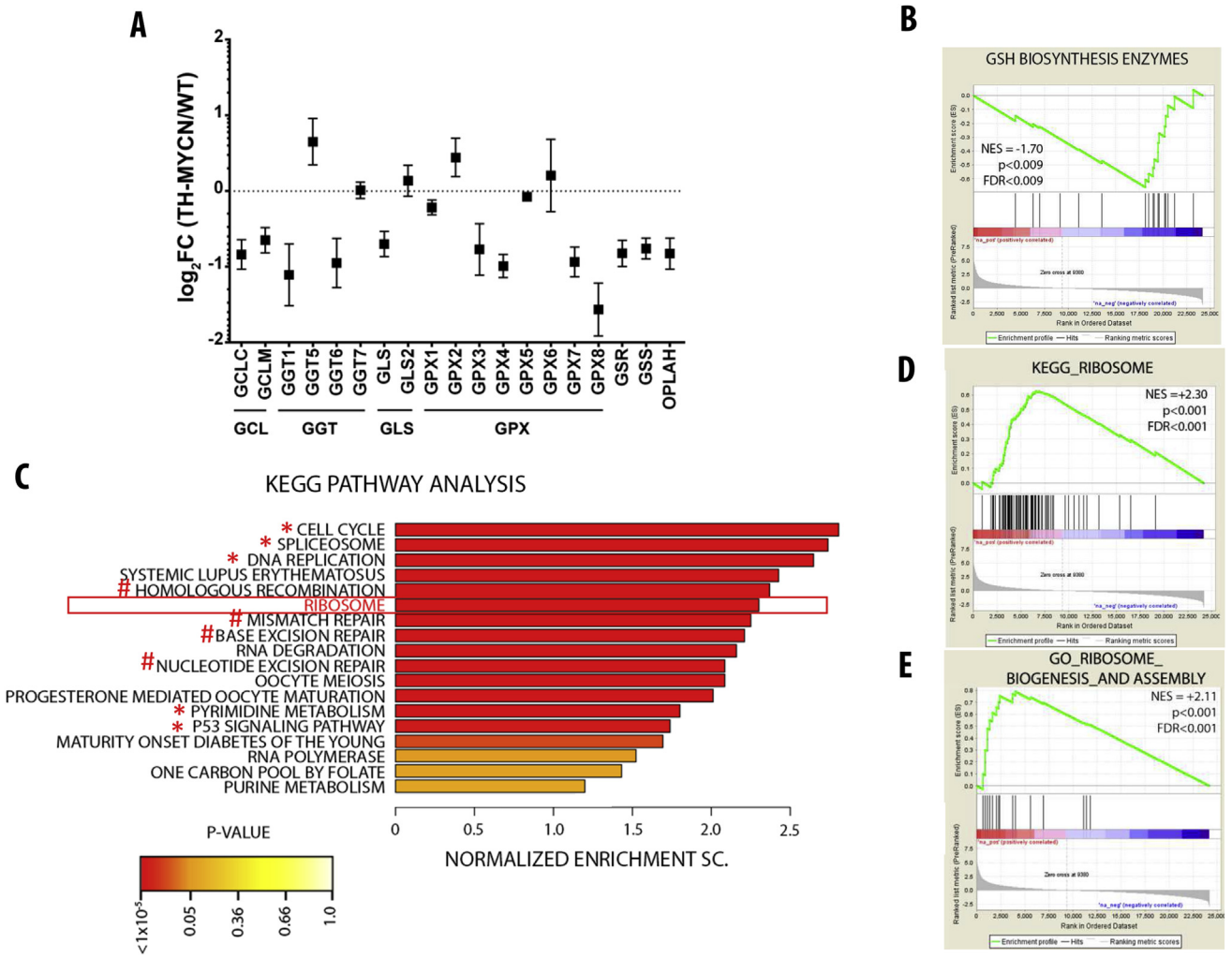

Figure 3 – Ribosomal biogenesis genes rather than glutathione biosynthesis enzymes are upregulated in pre-malignant *TH-MYCN* ganglia. A) Relative gene expression of enzymes involved in the glutathione biosynthesis pathway. Data is log_2 adjusted fold change for 2 week old *TH-MYCN* sympathetic ganglia compared to age matched wild-type ganglia. Data displayed indicates the average fold change in *TH-MYCN*$^{+/+}$ gene expression ± standard deviation from 6 independent ganglia. GLS, glutaminase, GCL, glutamyl-cysteine ligase, GPX, glutathione peroxidase, GSR, glutathione reductase, GGT, gamma-glutamyl transpeptidase, GSS; glutathione synthetase, OPLAH, 5-Oxoprolinase ATP-Hydrolyzing. B) Gene set enrichment plot for genes as displayed in A. Genes were analyzed by gene set enrichment analysis on a fold change ranked gene expression dataset comparing *TH-MYCN*$^{+/+}$ to wild-type ganglia derived from 2 week old mice. NES, normalized enrichment score, FDR, false discovery rate. C) Positively enriched gene sets from the KEGG database determined using gene set enrichment analysis on a fold change ranked gene expression dataset comparing *TH-MYCN*$^{+/+}$ to wild-type ganglia derived from 2 week old mice. Red box indicates the "KEGG_Ribosome" gene set. * indicates gene sets related to cell cycle/biogenesis. # indicates gene sets related to DNA repair. Only pathways with a p-value less than 0.1 are shown. Refer to Supplementary Table S5 for full analysis. D) Gene set enrichment plot for the "KEGG_Ribosome" as analyzed in C. E) Gene set enrichment plot for the gene ontology gene set termed "GO_Ribosome_Biogenesis_and_Assembly" analyzed by gene set enrichment analysis on a fold change ranked gene expression dataset comparing *TH-MYCN*$^{+/+}$ to wild-type ganglia derived from 2 week old mice.

3.4. *Glutathione is required for cell survival at* TH-MYCN *tumor initiation*

Since we had identified that glutathione abundance is in excess throughout *TH-MYCN*$^{+/+}$ tumorigenesis, we examined the functional relevance to tumor initiation. We used primary ganglia cultures from pre-tumor 2 week old *TH-MYCN*$^{+/+}$ mice, compared with wildtype mice (Calao et al., 2012; Carter et al., 2015; Hansford et al., 2004). Compared to wildtype controls, *TH-MYCN*$^{+/+}$ ganglia cultures showed a marked resistance to oxidative stress induced by hydrogen peroxide (H_2O_2) (Figure 4A) and were significantly more sensitive to the glutathione biosynthesis inhibitor, buthionine sulfoximine (BSO) (Figure 4B). Moreover, depletion of L-glutamine, the upstream glutamyl substrate of glutathione, from the culture media was selectively toxic to *TH-MYCN*$^{+/+}$, compared to wildtype cultures (Figure 4C), whereas depletion of a negative control substrate, D-glucose showed no significant difference in toxicity (Figure 4D). Importantly, cell death in *TH-MYCN*$^{+/+}$ cultures induced by BSO could be rescued by

L-glutamine supplementation into the media, suggesting that excess substrate abundance can effectively restore the functionality of this pathway (Figure 4E). These findings could also be recapitulated *in vivo*, where intraperitoneal administration of BSO or glutamate inhibitor, BPTES (Robinson et al., 2007), into 1 week old *TH-MYCN*$^{+/-}$ mice on a 5 days schedule, significantly reduced the proportion of ganglia hyperplasia at 2 weeks of age compared to vehicle control (Figure 4F–G).

3.5. *Excess glutathione abundance is required for tumor progression but not tumor maintenance in* TH-MYCN$^{+/+}$ *mice*

Next we examined whether glutathione was required for different stages of *TH-MYCN*$^{+/+}$ tumorigenesis by treating mice with BSO. First, we treated pre-tumor 3 week old *TH-MYCN*$^{+/+}$ mice with BSO before palpable tumors were detected (5 days/week at 500 mg/kg/day). We found that inhibition of

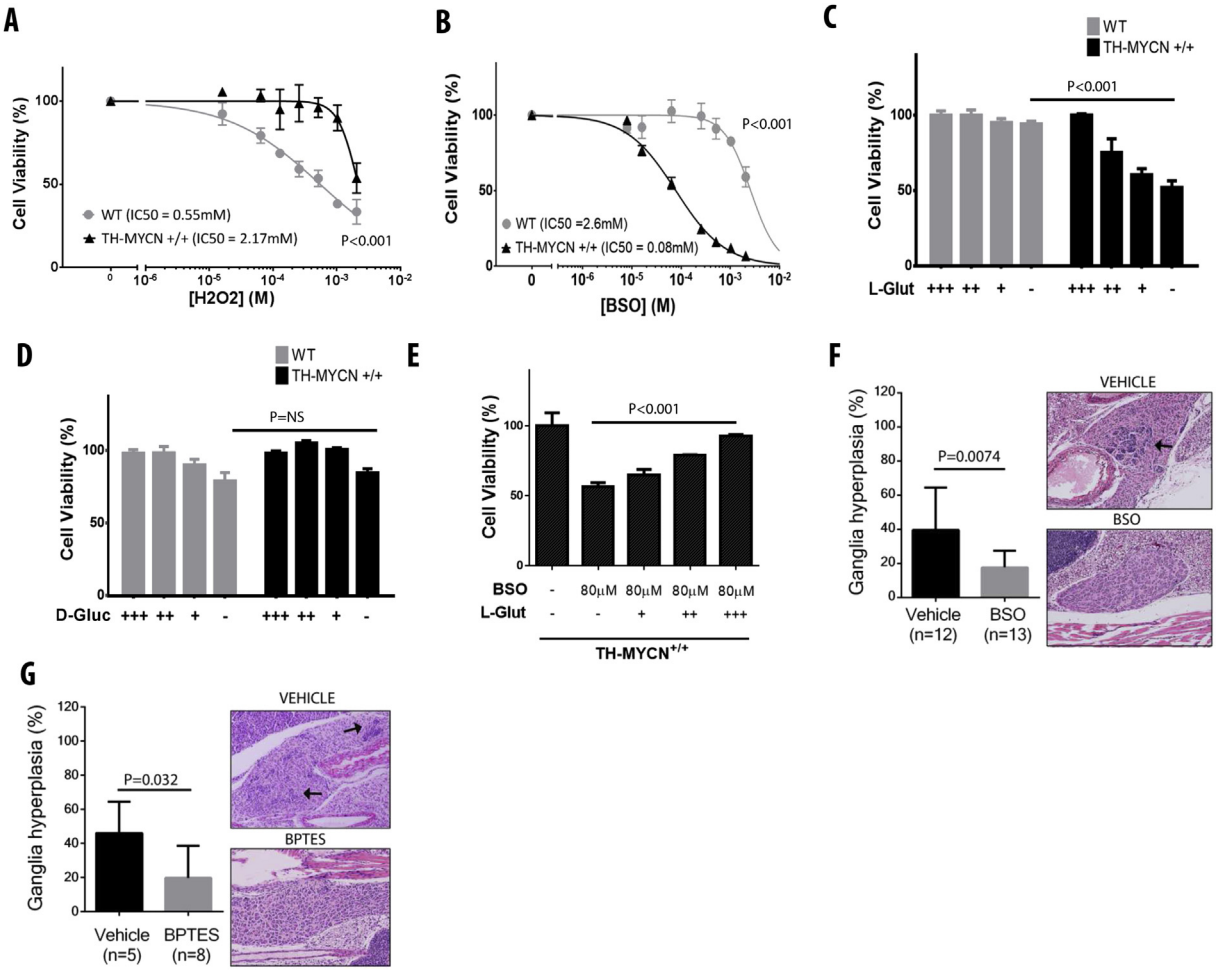

Figure 4 – Upregulation of glutathione biosynthesis enhances antioxidant activity and preserves cell viability in pre-malignant *TH-MYCN* ganglia. A) Primary sympathetic ganglia cultures derived from 2 week old pre-malignant *TH-MYCN*$^{+/+}$ mice and wild-type mice were treated with increasing concentrations of oxidative stress agent hydrogen peroxide (H_2O_2). Cell viability was evaluated using immunofluorescence by counting the total amount of βIII-tubulin positive cells (sympathetic neural lineage) and determining the percentage of viable cells compared to untreated cultures. Inhibitory concentration 50 was interpolated from non-linear regression curve. Cells were treated 48 h after cultures were seeded for a total of 48 h. Data displayed is average cell viability ± standard error derived from three independent biological replicates. P-value calculated using extra sum of squares F-test. B) Cell viability of primary sympathetic ganglia cultures treated as in A, except they were treated with increasing concentrations of glutathione biosynthesis inhibitor Buthionine sulfoximine (BSO). C) Cell viability of primary sympathetic ganglia cultures as in A, except they were treated by depriving L-glutamine (L-glut) from the growth media. +++; 0.5 mM, ++; 0.25 mM, +; 0.125 mM, −; 0 mM L-glutamine. D) Cell viability of primary sympathetic ganglia cultures as in A, except they were treated by depriving D-glucose (D-Gluc) from the growth media. +++; 25 mM, ++; 12.5 mM, +; 0.06125 mM, −; 0 mM D-glucose. NS; not significant. E) Cell viability of *TH-MYCN*$^{+/+}$ primary sympathetic ganglia cultures treated as in A, except they were treated with 80 μM of BSO and increasing supplementations of L-glutamine to the growth media. −; 0.5 mM, +; 1 mM, ++; 2 mM, +++; 4 mM L-glutamine. F) 6 day old *TH-MYCN*$^{+/-}$ mice were administered either intraperitoneal vehicle control (0.9% saline) or BSO (2.5 mmol/kg/day) for 5 days and the proportion of ganglia with hyperplastic neuroblasts was evaluated by histological examination. Ganglia were considered to be hyperplastic if > 30 focal neuroblasts were present per ganglion. Data displayed indicates the average proportion of hyperplastic ganglia per mouse ± standard deviation. Arrowheads indicate representative areas of neuroblast hyperplasia. G) As in F, except glutamate inhibitor bis-2-(5-phenylacetamido-1,2,4-thiadiazol-2-yl)ethyl sulfide 3 (BPTES) was used at 12.5 mg/kg/day.

glutathione biosynthesis at this time led to significant delays in tumor onset compared to vehicle-treated mice (Figure 5A). Next we treated mice with BSO after palpable tumors were detected (~4–5 weeks of age), but in this case, BSO alone had no effect on tumor growth compared to vehicle control (Figure 5B). However, BSO maintained its inhibitory effect when combined with chemotherapeutic agent vincristine compared to vincristine alone (Figure 5C). Taken together our results suggest that excess glutathione is a major requirement at tumor initiation in *TH-MYCN* mice, but once the tumor progresses it is only under chemotherapeutic stress that is it again required for tumor maintenance.

4. Discussion

MYC proteins have been closely associated with deregulation of metabolism in cancer cells (Cairns et al., 2011; Dang et al., 2009). However, whether MYC-dependent metabolic reprogramming is an early or late adaptation during tumorigenesis is unresolved. Here we used a MYCN-dependent mouse model of neuroblastoma to decipher altered metabolic pathways during different stages of tumorigenesis. We have shown that glutathione biosynthesis was upregulated early in pre-malignant sympathetic ganglia. As tumorigenesis progressed, the pathway was progressively enhanced to meet the demands of tumorigenesis. Correspondingly, expression of ribosomal biogenesis genes and upstream substrates of glutathione biosynthesis were markedly upregulated to lead to pathway overactivity. This suggests a hypothetical model in which pre-malignant ganglia with hyperplastic neuroblasts have increased resistance to oxidative stress as a result of increased glutathione abundance, and are dependent on substrate driven glutathione biosynthesis for cell survival and tumor progression (Figure 5D).

Our metabolomics analysis revealed that cell metabolism was generally upregulated during neuroblastoma tumorigenesis, with the vast majority of metabolites having increased abundance compared to age matched wildtype sympathetic ganglia. This was an expected finding, as cancer cells are well known to have overall higher metabolic activity due to their rapid proliferation and changing microenvironment (Cairns et al., 2011). Hence we focused our analysis on the most upregulated metabolites during *TH-MYCN*$^{+/+}$ tumorigenesis to identify drivers of tumor initiation. However, while this was our focus, there are some metabolites of note that were down-regulated over the course of tumor development, such as the mono- and disaccharides, glucose, ribose, maltose and sucrose. As cancer cells are well known to require simple sugars like glucose to meet their energy and macromolecule

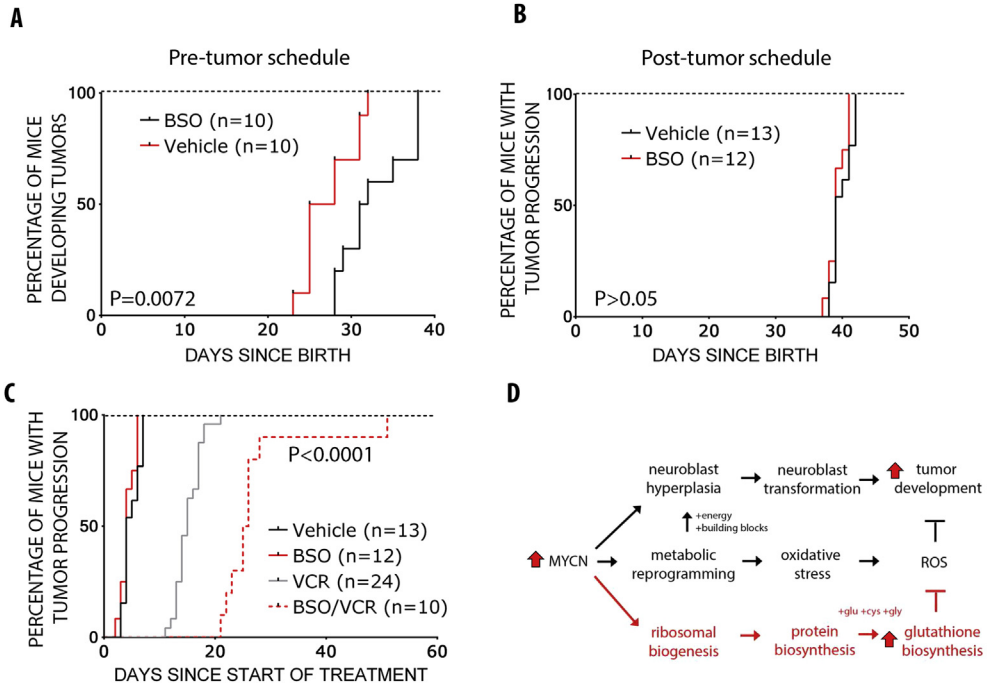

Figure 5 – Inhibition of glutathione biosynthesis delays tumor onset and sensitizes to vincristine chemotherapy in *TH-MYCN* mice. A) Three week old *TH-MYCN*$^{+/+}$ mice were administered either vehicle control (0.9% saline) or BSO (500 mg/kg/day) by gavage for 5 days/week and mice were monitored for detection of tumors by palpation. Graph displays the Kaplan–Meier analysis of time to first detection of tumors. P-value calculated by log-rank test. B) At the detection of 5 mm diameter tumors by palpation, ~4–5 week old *TH-MYCN*$^{+/+}$ mice were administered either vehicle control (0.9% saline) or BSO (500 mg/kg/day) by gavage for 5 days and mice were monitored for tumor growth by palpation. Graph displays the Kaplan–Meier analysis of time until tumors grow to 10 mm diameter. P-value calculated by log-rank test. C) As in B, except additional drug administration schedules for vincristine alone (VCR) and combination VCR/BSO are included. VCR was administered by intraperitoneal injection (0.2 mg/kg/day) for 5 days when 5 mm diameter tumors were detected by palpation in ~4–5 week old *TH-MYCN*$^{+/+}$ mice. P-value applies to the comparison between VCR/BSO and VCR alone. D) Hypothetical model of MYCN dependent metabolic reprogramming in *TH-MYCN* tumorigenesis. ROS; reactive oxygen species, glu; glutamate, cys; cysteine, gly; glycine.

biosynthesis demands, this was somewhat surprising. But considering that downstream substrates such as glucose-6-phosphate, fructose-6-phosphate, 3-phosphoglycerate, and lactate were all upregulated in *TH-MYCN*$^{+/+}$ ganglia/tumors this is more likely representative of glucose consumption, feeding into aerobic glycolysis (a well-studied cancer specific metabolic alteration commonly known as the "Warburg effect") (Cairns et al., 2011; Warburg, 1956). While formal proof of the aerobic glycolysis at neuroblastoma initiation is still required, this emphasizes the value of taking a pathway level view of metabolomics data.

We identified that metabolites involved in glutathione biosynthesis were markedly upregulated during *TH-MYCN*$^{+/+}$ tumorigenesis. However in parallel, we also showed that gene expression levels of enzymes involved in glutathione biosynthesis were downregulated at tumor initiation, contrasting with previous reports based on human tumor cell lines derived from established neuroblastomas (Veas-Perez de Tudela et al., 2010; Xiao et al., 2015). The reason for this inverse relationship between the substrates and enzymes of the glutathione pathway is unclear but it is possible that at this early stage of tumorigenesis, pre-malignant cells still maintain negative feedback control systems that repress enzyme expression in an attempt to control pathway overactivity. In contrast, ribosomal biogenesis genes were markedly upregulated in *TH-MYCN*$^{+/+}$ pre-tumor ganglia. Together with our metabolomics data identifying upregulation of protein biosynthesis in *TH-MYCN*$^{+/+}$ mice, this suggests that one of the earliest aberrations of MYCN deregulation through tumorigenesis is upregulation of ribosomal activity, increased translation of proteins and upregulation of the amino acids required for glutathione biosynthesis. Consistent with these conclusions, *TH-MYCN*$^{+/+}$ ganglia cultures required high levels of upstream glutamine for survival, and substrate supplementation could successfully rescue the toxicity of BSO mediated glutamyl-cysteine ligase inhibition. Our data suggest the rate-limiting step in glutathione biosynthesis at this early stage of tumorigenesis is upstream substrate abundance, as opposed enzyme expression. It is important to note though, that since BSO and BPTES were selectively toxic toward *TH-MYCN* ganglia *in vitro* and *in vivo*, there is still a requirement for enzyme expression to a certain threshold. Also, while ribosomal biogenesis can theoretically increase the protein pool required to supply the amino acids for glutathione biosynthesis, functional experiments are required to determine if upregulation of ribosomal genes is indeed critical for glutathione production.

We used *in vivo* drug administration experiments using inhibitors of glutathione biosynthesis to decipher the biological role of glutathione upregulation through *TH-MYCN* tumorigenesis. Consistent with a previous study on breast cancer, lymphoma and sarcoma (Harris et al., 2015), inhibition of the glutathione pathway was much more potent when administered before tumors had formed compared with treatment schedules against established tumors. Previously it has been reported that upregulation of compensatory antioxidant systems in established tumors such as the thioredoxin pathway or cystine import were responsible for this resistance to glutathione depletion (Harris et al., 2015). Future work will explore whether a similar mechanism explains resistance of established neuroblastomas to glutathione depletion. This may also explain why glutathione depletion is not sufficient to completely prevent tumor progression in several cancer model systems (Harris et al., 2015). With this knowledge, potential chemo-preventative or metabolic modification therapies may be developed that impair aberrant antioxidant activity to prevent or reduce cancer incidence. Regardless, these findings suggest caution should be exercised when considering high antioxidant maternal diets during pregnancy.

Contrasting with our single agent experiments with BSO, we showed that BSO markedly delayed tumor growth of established neuroblastomas when administered as a combination therapy with vincristine, a commonly used chemotherapeutic for neuroblastoma patients. It is currently unclear if this increased efficacy can be attributed to previously reported role of vincristine in inducing reactive oxygen species (Chen et al., 2011; Groninger et al., 2002; Simizu et al., 1998; Tsai et al., 2007) or if an independent mechanism explains the combination activity of vincristine and BSO. For instance, MYCN downstream target gene MRP1 mediates resistance to vincristine by glutathione-dependent drug efflux, so it is possible glutathione inhibition with BSO may impair this process indirectly and potentiate vincristine cytotoxicity (Burkhart et al., 2009; Loe et al., 1998; Schneider et al., 1995). Nevertheless, our data suggest that the upregulation of glutathione biosynthesis during MYCN-driven neuroblastoma tumorigenesis could potentially be exploited therapeutically as an adjuvant to increase potency of existing therapies. Moreover, identification of novel and potent combinatorial interactions between glutathione-targeted and other anticancer agents should be investigated.

Here we present a hypothesis that the MYCN oncogenic role in enhancing ribosomal gene expression may be the mechanism that provides upstream substrates to drive glutathione biosynthesis at tumor initiation. Notably, high glutathione levels have also been shown to be required for the initiation of adult cancers of diverse oncogenic stimuli, such as PyMT overexpression, KRAS activation or PTEN knockout (Harris et al., 2015). Thus, it seems likely that a requirement for glutathione during tumorigenesis is a shared feature of different oncogenic drivers in cancer, but whether the mechanism of glutathione biosynthesis is associated with excess ribosomal activity and substrate abundance is yet to be determined. Further work will evaluate if ribosomal activity is an absolute requirement for glutathione biosynthesis at the initiation of neuroblastoma and other cancers. This will not only reveal the sequence of events in cancer initiation but will inform novel metabolic targeted therapies that potentially inhibit both ribosomal and antioxidant activity.

5. Conclusions

Here we have conducted a metabolomics analysis in an animal model of MYCN-driven neuroblastoma tumorigenesis. We showed that upregulation of glutathione biosynthesis is an important early change in metabolism that allows for cell survival at the initiation of neuroblastoma. Future work should focus on the relevance of these findings to human

patients, in particular whether novel therapeutics targeting aberrant glutathione and antioxidant activity can be developed for prevention or treatment of neuroblastoma.

Acknowledgments

We thank Dr. Andrew Gifford (Department of Anatomical Pathology, Prince of Wales Hospital, Australia) for histopathological advice on sympathetic ganglia analysis.

Funding

This work was supported by a Project grant from The Balnaves Foundation Young Researchers Fund and Program Grants from the NHMRC Australia (grant number APP1016699); Cancer Institute NSW (grant number 10/TPG/1-03); and Cancer Council NSW (grant numbers PG-11-06).

Author contributions

D.R.C., B.B.C, G.M.M conceived the project. D.R.C, B.B.C, G.M.M supervised the project. M.H, M.D.N, R.E.G and J.I.F were advisors for the project. F.S, K.D.P, A.B supplied mouse gene expression data. D.R.C, S.K.S, M.P, J.M, E.S designed, performed and analyzed experiments. D.R.C, B.B.C, G.M.M wrote the manuscript.

Conflict of interest

The authors declare no potential conflict of interests.

Data and materials availability

Gene expression data for 2 week old *TH-MYCN*$^{+/+}$ and wild-type ganglia is available at the Gene Expression Omnibus under accession # GSE71105.

Appendix A. Supplementary data

Supplementary data related to this article can be found at http://dx.doi.org/10.1016/j.molonc.2016.02.004.

REFERENCES

Alam, G., Cui, H., Shi, H., Yang, L., Ding, J., Mao, L., Maltese, W.A., Ding, H.F., 2009. MYCN promotes the expansion of Phox2B-positive neuronal progenitors to drive neuroblastoma development. Am. J. Pathol. 175, 856–866.

Beckwith, J.B., Perrin, E.V., 1963. In situ neuroblastomas: a contribution to the natural history of neural crest tumors. Am. J. Pathol. 43, 1089–1104.

Benassi, B., Fanciulli, M., Fiorentino, F., Porrello, A., Chiorino, G., Loda, M., Zupi, G., Biroccio, A., 2006. c-Myc phosphorylation is required for cellular response to oxidative stress. Mol. Cell 21, 509–519.

Brockmann, M., Poon, E., Berry, T., Carstensen, A., Deubzer, H.E., Rycak, L., Jamin, Y., Thway, K., Robinson, S.P., Roels, F., Witt, O., Fischer, M., Chesler, L., Eilers, M., 2013. Small molecule inhibitors of aurora-a induce proteasomal degradation of N-myc in childhood neuroblastoma. Cancer Cell 24, 75–89.

Brodeur, G.M., 2003. Neuroblastoma: biological insights into a clinical enigma. Nat. Rev. Cancer 3, 203–216.

Brodeur, G.M., Seeger, R.C., Schwab, M., Varmus, H.E., Bishop, J.M., 1984. Amplification of N-myc in untreated human neuroblastomas correlates with advanced disease stage. Science 224, 1121–1124.

Burkhart, C.A., Watt, F., Murray, J., Pajic, M., Prokvolit, A., Xue, C., Flemming, C., Smith, J., Purmal, A., Isachenko, N., Komarov, P.G., Gurova, K.V., Sartorelli, A.C., Marshall, G.M., Norris, M.D., Gudkov, A.V., Haber, M., 2009. Small-molecule multidrug resistance-associated protein 1 inhibitor reversan increases the therapeutic index of chemotherapy in mouse models of neuroblastoma. Cancer Res. 69, 6573–6580.

Cairns, R.A., Harris, I.S., Mak, T.W., 2011. Regulation of cancer cell metabolism. Nat. Rev. Cancer 11, 85–95.

Calao, M., Sekyere, E.O., Cui, H.J., Cheung, B.B., Thomas, W.D., Keating, J., Chen, J.B., Raif, A., Jankowski, K., Davies, N.P., Bekkum, M.V., Chen, B., Tan, O., Ellis, T., Norris, M.D., Haber, M., Kim, E.S., Shohet, J.M., Trahair, T.N., Liu, T., Wainwright, B.J., Ding, H.F., Marshall, G.M., 2012. Direct effects of Bmi1 on p53 protein stability inactivates oncoprotein stress responses in embryonal cancer precursor cells at tumor initiation. Oncogene 32, 3616–3626.

Carter, D.R., Murray, J., Cheung, B.B., Gamble, L., Koach, J., Tsang, J., Sutton, S., Kalla, H., Syed, S., Gifford, A.J., Issaeva, N., Biktasova, A., Atmadibrata, B., Sun, Y., Sokolowski, N., Ling, D., Kim, P.Y., Webber, H., Clark, A., Ruhle, M., Liu, B., Oberthuer, A., Fischer, M., Byrne, J., Saletta, F., Thwe le, M., Purmal, A., Haderski, G., Burkhart, C., Speleman, F., De Preter, K., Beckers, A., Ziegler, D.S., Liu, T., Gurova, K.V., Gudkov, A.V., Norris, M.D., Haber, M., Marshall, G.M., 2015. Therapeutic targeting of the MYC signal by inhibition of histone chaperone FACT in neuroblastoma. Sci. Transl. Med. 7, 312ra176.

Chen, M.B., Shen, W.X., Yang, Y., Wu, X.Y., Gu, J.H., Lu, P.H., 2011. Activation of AMP-activated protein kinase is involved in vincristine-induced cell apoptosis in B16 melanoma cell. J. Cell. Physiol. 226, 1915–1925.

Chesler, L., Weiss, W.A., 2011. Genetically engineered murine models–contribution to our understanding of the genetics, molecular pathology and therapeutic targeting of neuroblastoma. Semin. Cancer Biol. 21, 245–255.

Chipumuro, E., Marco, E., Christensen, C.L., Kwiatkowski, N., Zhang, T., Hatheway, C.M., Abraham, B.J., Sharma, B., Yeung, C., Altabef, A., Perez-Atayde, A., Wong, K.K., Yuan, G.C., Gray, N.S., Young, R.A., George, R.E., 2014. CDK7 inhibition suppresses super-enhancer-linked oncogenic transcription in MYCN-driven cancer. Cell 159, 1126–1139.

Dang, C.V., Kim, J.W., Gao, P., Yustein, J., 2008. The interplay between MYC and HIF in cancer. Nat. Rev. Cancer 8, 51–56.

Dang, C.V., Le, A., Gao, P., 2009. MYC-induced cancer cell energy metabolism and therapeutic opportunities. Clin. Cancer Res. Off. J. Am. Assoc. Cancer Res. 15, 6479–6483.

David, C.J., Chen, M., Assanah, M., Canoll, P., Manley, J.L., 2010. HnRNP proteins controlled by c-Myc deregulate pyruvate kinase mRNA splicing in cancer. Nature 463, 364–368.

Frolkis, A., Knox, C., Lim, E., Jewison, T., Law, V., Hau, D.D., Liu, P., Gautam, B., Ly, S., Guo, A.C., Xia, J., Liang, Y., Shrivastava, S., Wishart, D.S., 2010. SMPDB: the small molecule pathway database. Nucleic Acids Res. 38, D480–D487.

Gao, P., Tchernyshyov, I., Chang, T.C., Lee, Y.S., Kita, K., Ochi, T., Zeller, K.I., De Marzo, A.M., Van Eyk, J.E., Mendell, J.T., Dang, C.V., 2009. c-Myc suppression of miR-23a/b enhances mitochondrial glutaminase expression and glutamine metabolism. Nature 458, 762–765.

Groninger, E., Meeuwsen-De Boer, G.J., De Graaf, S.S., Kamps, W.A., De Bont, E.S., 2002. Vincristine induced apoptosis in acute lymphoblastic leukaemia cells: a mitochondrial controlled pathway regulated by reactive oxygen species? Int. J. Oncol. 21, 1339–1345.

Hansford, L.M., Thomas, W.D., Keating, J.M., Burkhart, C.A., Peaston, A.E., Norris, M.D., Haber, M., Armati, P.J., Weiss, W.A., Marshall, G.M., 2004. Mechanisms of embryonal tumor initiation: distinct roles for MycN expression and MYCN amplification. Proc. Natl. Acad. Sci. U S A 101, 12664–12669.

Harris, I.S., Treloar, A.E., Inoue, S., Sasaki, M., Gorrini, C., Lee, K.C., Yung, K.Y., Brenner, D., Knobbe-Thomsen, C.B., Cox, M.A., Elia, A., Berger, T., Cescon, D.W., Adeoye, A., Brustle, A., Molyneux, S.D., Mason, J.M., Li, W.Y., Yamamoto, K., Wakeham, A., Berman, H.K., Khokha, R., Done, S.J., Kavanagh, T.J., Lam, C.W., Mak, T.W., 2015. Glutathione and thioredoxin antioxidant pathways synergize to drive cancer initiation and progression. Cancer Cell 27, 211–222.

Henderson, M.J., Haber, M., Porro, A., Munoz, M.A., Iraci, N., Xue, C., Murray, J., Flemming, C.L., Smith, J., Fletcher, J.I., Gherardi, S., Kwek, C.K., Russell, A.J., Valli, E., London, W.B., Buxton, A.B., Ashton, L.J., Sartorelli, A.C., Cohn, S.L., Schwab, M., Marshall, G.M., Perini, G., Norris, M.D., 2011. ABCC multidrug transporters in childhood neuroblastoma: clinical and biological effects independent of cytotoxic drug efflux. J. Natl. Cancer Inst. 103, 1236–1251.

Kim, J.W., Gao, P., Liu, Y.C., Semenza, G.L., Dang, C.V., 2007. Hypoxia-inducible factor 1 and dysregulated c-Myc cooperatively induce vascular endothelial growth factor and metabolic switches hexokinase 2 and pyruvate dehydrogenase kinase 1. Mol. Cell. Biol. 27, 7381–7393.

Le, A., Lane, A.N., Hamaker, M., Bose, S., Gouw, A., Barbi, J., Tsukamoto, T., Rojas, C.J., Slusher, B.S., Zhang, H., Zimmerman, L.J., Liebler, D.C., Slebos, R.J., Lorkiewicz, P.K., Higashi, R.M., Fan, T.W., Dang, C.V., 2012. Glucose-independent glutamine metabolism via TCA cycling for proliferation and survival in B cells. Cell Metab. 15, 110–121.

Loe, D.W., Deeley, R.G., Cole, S.P., 1998. Characterization of vincristine transport by the M(r) 190,000 multidrug resistance protein (MRP): evidence for cotransport with reduced glutathione. Cancer Res. 58, 5130–5136.

Maris, J.M., 2010. Recent advances in neuroblastoma. New Engl. J. Med. 362, 2202–2211.

Marshall, G.M., Carter, D.R., Cheung, B.B., Liu, T., Mateos, M.K., Meyerowitz, J.G., Weiss, W.A., 2014. The prenatal origins of cancer. Nat. Rev. Cancer 14, 277–289.

Mohlin, S., Hamidian, A., von Stedingk, K., Bridges, E., Wigerup, C., Bexell, D., Pahlman, S., 2015. PI3K-mTORC2 but not PI3K-mTORC1 regulates transcription of HIF2A/EPAS1 and vascularization in neuroblastoma. Cancer Res. 75, 4617–4628.

Mootha, V.K., Lindgren, C.M., Eriksson, K.F., Subramanian, A., Sihag, S., Lehar, J., Puigserver, P., Carlsson, E., Ridderstrale, M., Laurila, E., Houstis, N., Daly, M.J., Patterson, N., Mesirov, J.P., Golub, T.R., Tamayo, P., Spiegelman, B., Lander, E.S., Hirschhorn, J.N., Altshuler, D., Groop, L.C., 2003. PGC-1alpha-responsive genes involved in oxidative phosphorylation are coordinately downregulated in human diabetes. Nat. Genet. 34, 267–273.

Ogata, H., Goto, S., Sato, K., Fujibuchi, W., Bono, H., Kanehisa, M., 1999. KEGG: Kyoto encyclopedia of genes and genomes. Nucleic Acids Res. 27, 29–34.

Puissant, A., Frumm, S.M., Alexe, G., Bassil, C.F., Qi, J., Chanthery, Y.H., Nekritz, E.A., Zeid, R., Gustafson, W.C., Greninger, P., Garnett, M.J., McDermott, U., Benes, C.H., Kung, A.L., Weiss, W.A., Bradner, J.E., Stegmaier, K., 2013. Targeting MYCN in neuroblastoma by BET bromodomain inhibition. Cancer Discov. 3, 308–323.

Reitman, Z.J., Jin, G., Karoly, E.D., Spasojevic, I., Yang, J., Kinzler, K.W., He, Y., Bigner, D.D., Vogelstein, B., Yan, H., 2011. Profiling the effects of isocitrate dehydrogenase 1 and 2 mutations on the cellular metabolome. Proc. Natl. Acad. Sci. U S A 108, 3270–3275.

Robinson, M.M., McBryant, S.J., Tsukamoto, T., Rojas, C., Ferraris, D.V., Hamilton, S.K., Hansen, J.C., Curthoys, N.P., 2007. Novel mechanism of inhibition of rat kidney-type glutaminase by bis-2-(5-phenylacetamido-1,2,4-thiadiazol-2-yl)ethyl sulfide (BPTES). Biochem. J. 406, 407–414.

Schneider, E., Yamazaki, H., Sinha, B.K., Cowan, K.H., 1995. Buthionine sulfoximine-mediated sensitisation of etoposide-resistant human breast cancer MCF7 cells overexpressing the multidrug resistance-associated protein involves increased drug accumulation. Br. J. Cancer 71, 738–743.

Schwab, M., Alitalo, K., Klempnauer, K.H., Varmus, H.E., Bishop, J.M., Gilbert, F., Brodeur, G., Goldstein, M., Trent, J., 1983. Amplified DNA with limited homology to myc cellular oncogene is shared by human neuroblastoma cell lines and a neuroblastoma tumour. Nature 305, 245–248.

Schwab, M., Ellison, J., Busch, M., Rosenau, W., Varmus, H.E., Bishop, J.M., 1984. Enhanced expression of the human gene N-myc consequent to amplification of DNA may contribute to malignant progression of neuroblastoma. Proc. Natl. Acad. Sci. U S A 81, 4940–4944.

Simizu, S., Takada, M., Umezawa, K., Imoto, M., 1998. Requirement of caspase-3(-like) protease-mediated hydrogen peroxide production for apoptosis induced by various anticancer drugs. J. Biol. Chem. 273, 26900–26907.

Subramanian, A., Tamayo, P., Mootha, V.K., Mukherjee, S., Ebert, B.L., Gillette, M.A., Paulovich, A., Pomeroy, S.L., Golub, T.R., Lander, E.S., Mesirov, J.P., 2005. Gene set enrichment analysis: a knowledge-based approach for interpreting genome-wide expression profiles. Proc. Natl. Acad. Sci. U S A 102, 15545–15550.

Tsai, S.Y., Sun, N.K., Lu, H.P., Cheng, M.L., Chao, C.C., 2007. Involvement of reactive oxygen species in multidrug resistance of a vincristine-selected lymphoblastoma. Cancer Sci. 98, 1206–1214.

van Riggelen, J., Yetil, A., Felsher, D.W., 2010. MYC as a regulator of ribosome biogenesis and protein synthesis. Nat. Rev. Cancer 10, 301–309.

Veas-Perez de Tudela, M., Delgado-Esteban, M., Cuende, J., Bolanos, J.P., Almeida, A., 2010. Human neuroblastoma cells with MYCN amplification are selectively resistant to oxidative stress by transcriptionally up-regulating glutamate cysteine ligase. J. Neurochem. 113, 819–825.

Warburg, O., 1956. On the origin of cancer cells. Science 123, 309–314.

Weiss, W.A., Aldape, K., Mohapatra, G., Feuerstein, B.G., Bishop, J.M., 1997. Targeted expression of MYCN causes neuroblastoma in transgenic mice. EMBO J. 16, 2985–2995.

Xia, J., Wishart, D.S., 2010. MSEA: a web-based tool to identify biologically meaningful patterns in quantitative metabolomic data. Nucleic Acids Res. 38, W71–W77.

Xiao, D., Ren, P., Su, H., Yue, M., Xiu, R., Hu, Y., Liu, H., Qing, G., 2015. Myc promotes glutaminolysis in human neuroblastoma through direct activation of glutaminase 2. Oncotarget.

Zimmerman, K.A., Yancopoulos, G.D., Collum, R.G., Smith, R.K., Kohl, N.E., Denis, K.A., Nau, M.M., Witte, O.N., Toran-Allerand, D., Gee, C.E., et al., 1986. Differential expression of myc family genes during murine development. Nature 319, 780–783.